AFRL-RY-WP-TR-2020-0175

VERTICAL-CAVITY SURFACE-EMITTING PHASE SHIFTER (VCSEP)

Y. Fainman
University of California San Diego

JUNE 2020
Final Report

Approved for public release; distribution is unlimited.

See additional restrictions described on inside pages

STINFO COPY

AIR FORCE RESEARCH LABORATORY
SENSORS DIRECTORATE
WRIGHT-PATTERSON AIR FORCE BASE, OH 45433-7320
AIR FORCE MATERIEL COMMAND
UNITED STATES AIR FORCE

NOTICE AND SIGNATURE PAGE

Using Government drawings, specifications, or other data included in this document for any purpose other than Government procurement does not in any way obligate the U.S. Government. The fact that the Government formulated or supplied the drawings, specifications, or other data does not license the holder or any other person or corporation; or convey any rights or permission to manufacture, use, or sell any patented invention that may relate to them.

This report is the result of contracted fundamental research deemed exempt from public affairs security and policy review in accordance with The Under Secretary of Defense memorandum dated 24 May 2010 and AFRL/DSO policy clarification email dated 13 January 2020. This report is available to the general public, including foreign nationals.

Copies may be obtained from the Defense Technical Information Center (DTIC) (http://www.dtic.mil).

AFRL-RY-WP-TR-2020-0175 HAS BEEN REVIEWED AND IS APPROVED FOR PUBLICATION IN ACCORDANCE WITH ASSIGNED DISTRIBUTION STATEMENT.

*//Signature//

NICHOLAS G. USECHAK
Program Manager
Highly Integrated Microsystems Branch
Aerospace Components & Subsystems Division

//Signature//

ATTILA A. SZEP, Chief
Highly Integrated Microsystems Branch
Aerospace Components & Subsystems Division

//Signature//

ADAM L. BROOKS, Lt Col, USAF
Deputy
Aerospace Components & Subsystems Division
Sensors Directorate

This report is published in the interest of scientific and technical information exchange, and its publication does not constitute the Government's approval or disapproval of its ideas or findings.

*Disseminated copies will show "//Signature//" stamped or typed above the signature blocks.

REPORT DOCUMENTATION PAGE

Form Approved
OMB No. 0704-0188

1. REPORT DATE *(DD-MM-YY)*	2. REPORT TYPE	3. DATES COVERED *(From - To)*
June 2020	Final	19 January 2018 – 19 January 2020

4. TITLE AND SUBTITLE
VERTICAL-CAVITY SURFACE-EMITTING PHASE SHIFTER (VCSEP)

5a. CONTRACT NUMBER
FA8650-18-1-7816

5b. GRANT NUMBER

5c. PROGRAM ELEMENT NUMBER
62716E

6. AUTHOR(S)
Y. Fainman

5d. PROJECT NUMBER
N/A

5e. TASK NUMBER
N/A

5f. WORK UNIT NUMBER
Y1QJ

7. PERFORMING ORGANIZATION NAME(S) AND ADDRESS(ES)

University of California San Diego
9500 Gilman Dr.
La Jolla, CA 92093

8. PERFORMING ORGANIZATION REPORT NUMBER
AFRL-RY-WP-TR-2020-0175

9. SPONSORING/MONITORING AGENCY NAME(S) AND ADDRESS(ES)

Air Force Research Laboratory
Sensors Directorate
Wright-Patterson Air Force Base, OH 45433-7320
Air Force Materiel Command
United States Air Force

Defense Advanced
Research Projects Agency
(DARPA/MTO)
675 North Randolph St.
Arlington, VA 22203

10. SPONSORING/MONITORING AGENCY ACRONYM(S)
AFRL/RYDI

11. SPONSORING/MONITORING AGENCY REPORT NUMBER(S)
AFRL-RY-WP-TR-2020-0175

12. DISTRIBUTION/AVAILABILITY STATEMENT
Approved for public release; distribution is unlimited.

13. SUPPLEMENTARY NOTES
This report is the result of contracted fundamental research deemed exempt from public affairs security and policy review in accordance with The Under Secretary of Defense memorandum dated 24 May 2010 and AFRL/DSO policy clarification email dated 13 January 2020. This material is based on research sponsored by Air Force Research laboratory (AFRL) and the Defense Advanced Research Agency (DARPA) under agreement number FA8650-18-1-7816. The U.S. Government is authorized to reproduce and distribute reprints for Governmental purposes notwithstanding any copyright notation herein. The views and conclusions contained herein are those of the authors and should not be interpreted as necessarily representing the official policies of endorsements, either expressed or implied, of AFRL and DARPA or the U.S. Government. Report contains color.

14. ABSTRACT
In this report, we investigate the Vertical Cavity Surface Emitting Phase-shifters (VCSEP) for the Modular Optical Aperture Building Blocks (MOABB) program. In this work we introduced a new concept for realization of phase shifters utilizing hybrid resonance structures in cylindrical topology leveraging our prior experience in nanoscale light emitters and nanolaser technology and developed novel design and simulation tools, nanofabrication procedures, and demonstrated devices with aspect ratios of 15:1.

15. SUBJECT TERMS
optical phased arrays, integrated photonics, beam steering, nano-photonics, micro-photonic pillars

16. SECURITY CLASSIFICATION OF:			17. LIMITATION OF ABSTRACT:	18. NUMBER OF PAGES	19a. NAME OF RESPONSIBLE PERSON (Monitor)
a. REPORT	b. ABSTRACT	c. THIS PAGE			Nicholas Usechak
Unclassified	Unclassified	Unclassified	SAR	37	19b. TELEPHONE NUMBER *(Include Area Code)* N/A

Table of Contents

Section **Page**

List of Figures

Figure **Page**

List of Tables

Tables **Page**

PREFACE

The authors would like to thank the technical and administrative support of the government team.

1. SUMMARY

The proposed research objective of this study was to advance the state of the art in support of the Modular Optical Aperture Building Blocks (MOABB) program by developing Vertical Cavity Surface Emitting Phase-shifters (VCSEP). In this work we (i) introduced a new concept for realization of phase shifters utilizing hybrid resonance structures in cylindrical topology leveraging our groups prior experience in nanoscale light emitters and nanolaser technology; (ii) we developed novel design and simulation tools, nanofabrication procedures, and demonstrated devices with aspect ratios of 15:1. These devices had diameters less than 1 μm (footprints <1 μm^2) enabling dense integration of VCSEP devices to achieve the ultimate goals of MOABB's wide angular scanning range (~120^0) with high resolution (~0.5^o) in two-dimensional (2D); (iii) we advanced the state of the art in complementary metal-oxide semiconductor (CMOS) compatible nonlinear optical materials such as silicon-rich silicon nitride for VCSEP applications. We also introduced the concept of direct current (DC) induced Pockels effect in CMOS compatible dielectrics which will advance numerous applications that rely on strong second-order nonlinear optical effects; (iv) we constructed two characterization and testing systems and developed novel characterization approaches that led to characterization of spectral response of single VCSEP device.

Based on the analysis of the current study the following recommendations for future work are offered: (i) continue investigation of VCSEP architecture for compact integrated scanners for light detection and ranging (LIDAR) applications; (ii) continue developing CMOS compatible nonlinear optical dielectric materials exploiting the DC induced Pockels effect for light modulation as well as nonlinear wave mixing that transfer information between different optical carrier waves. This includes a fundamental study of the nonlinear optical properties of dielectrics in strong DC electric fields, which are easily achievable in nanoscale devices at very low voltages.

2. INTRODUCTION

2.1 Background

Today optical beams are spatially scanned using laser sources coupled to free-space optical systems comprised of mechanical components, moving parts, and bulk optics. Unfortunately, the application range of these legacy systems is limited by their size, weight, reliability and cost. Consequently, a substantial research effort has been directed toward the miniaturization and simplification of these systems. Recent work has focused on beam steering using optical phased arrays.

Although optical phased arrays are an elegant non-mechanical beam steering approach, the technical and environmental challenges compared to radio frequency (RF) systems (optical systems use wavelengths 10,000 times smaller leading to difficult tolerances) are daunting. The main challenge to construct viable optical phased array base beam steering solutions relies on one's ability to construct ultra-compact phase shifters with footprints < 1 μm^2 and power consumptions < $5\mu W/2\pi$. Moreover, these phase shifters should enable scalability to large size 2D arrays with a period on the order of the wavelength of light to allow wide angular scanning range and high angular resolutions.

Currently, compact chip-scale 2D phased-array optics are implemented using 2D arrays of phase shifters based on waveguide-coupled directional gratings (Figure 1) [1]. These devices are based on a photonic architecture in which photonic waveguides feed a linear array of add/drop filters. The amount of coupling into each add/drop filter can be modulated thermally via metal heaters. From the add/drop, the light is passed to a grating which serves as a nanoantenna and emits the light vertically. Compact 64 x 64 arrays of phase shifters with a pixel size of 9 μm × 9 μm or 89 μm^2 have already been reported [1]. Such approaches are fundamentally limited in pixel size by the size of the waveguide couplers themselves, which due to the physical requirements of wavelength scaling, are necessarily longer than 1 μm, as seen in [1]. Likewise, the heaters add a non-negligible footprint requirement, in terms of both the physical size of the heaters themselves and the required thermal isolation, which mandates some separation from nearby pixels. Additionally, if response time becomes a concern, heaters have limitations there as well. It may be possible to control coupling in such devices via direct current injection, but even then, that approach would still be limited by the physical size of the waveguide coupler.

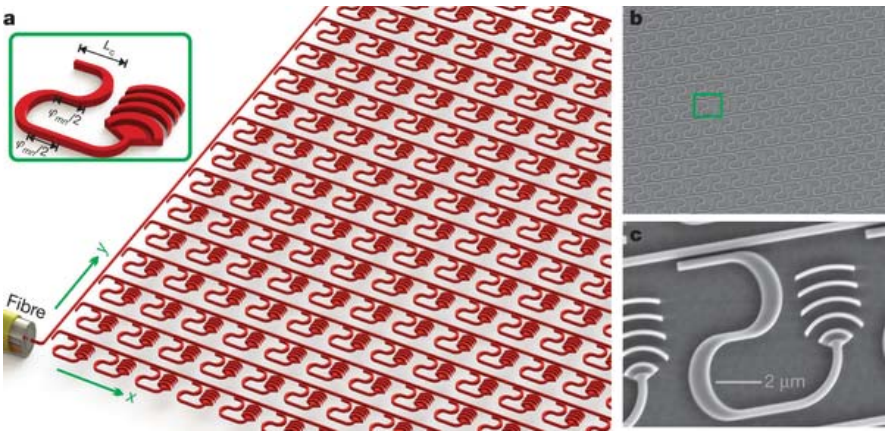

Figure 1: 2D Array of Phase Shifters Based on Waveguide Coupled Directional Gratings

To further advance the state of the art and achieve the ultimate performance metrics of phase shifter arrays for beam-forming applications, we propose an alternative approach to the creation of large 2D arrays of small footprint phase shifters. Our approach uses a 2D array of hybrid plasmonic resonators realized vertically with an input optical carrier inserted from an integrated bottom layer, which is modulated by a phase shifter and re-emitted in the vertical direction to form a beam in the far field. Since the waveguide distribution network of the optical carrier is feasible, this work focused on the challenge associated with creating a vertical hybrid plasmonic waveguide in a cylindrical topology to produce VCSEP. In the following, we describe our proposed design and optimization methodologies, discuss the necessary fabrication processes, and address various characterizations tasks to evaluate performances of the proposed VCSEP.

2.2 Approach

Our VCSEP approach is based on a vertical realization of a hybrid plasmonic waveguide in a cylindrical topology as depicted in Figure 2. To explain our approach, it is necessary to provide a brief overview of the techniques currently used in the areas of photonic cavity phase modulators, plasmonic phase modulators, and hybrid plasmonic phase modulators.

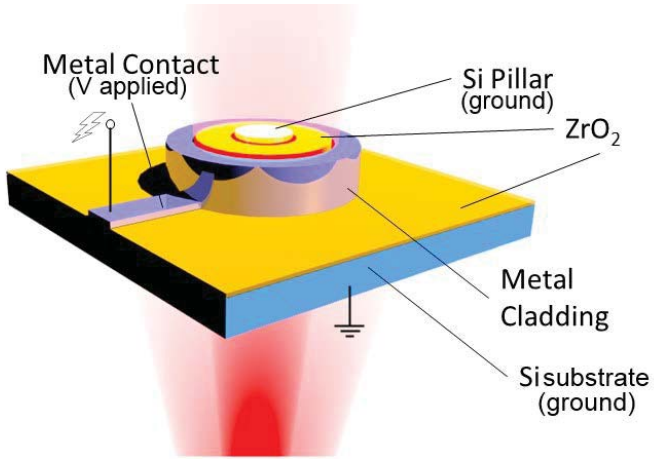

Figure 2: Schematic Diagram of the Proposed VCSEP Operating in Transmission Mode
Light enters through the bottom, is phase shifted, and exits topside.

Most compact phase modulators use either a photonic resonator design [2] or a plasmonic waveguide in a traveling-wave [1] or Mach–Zehnder [3] configuration. In the former case, a resonant cavity with a large quality factor is used to enhance the nonlinear interaction by several orders of magnitude. The effective interaction length is increased by having photons make multiple passes through a nonlinear material; using this method, devices as small as 78 μm^2 have been demonstrated [2]. In the latter case, photonic modes are coupled to localized high *k*-vector plasmonic modes; these higher k-vector plasmonic modes have the same frequency as the incident photonic mode but a much shorter effective wavelength. In effect, the interaction length in the nonlinear material is increased by "squeezing" the light in the direction of propagation [1,3,4] (see Figure 3). Plasmonic phase modulators with waveguide lengths of 12.5 µm and 10 µm [3,5] have been demonstrated, but total device footprint remains well above 50 μm^2 [1,3,5] .

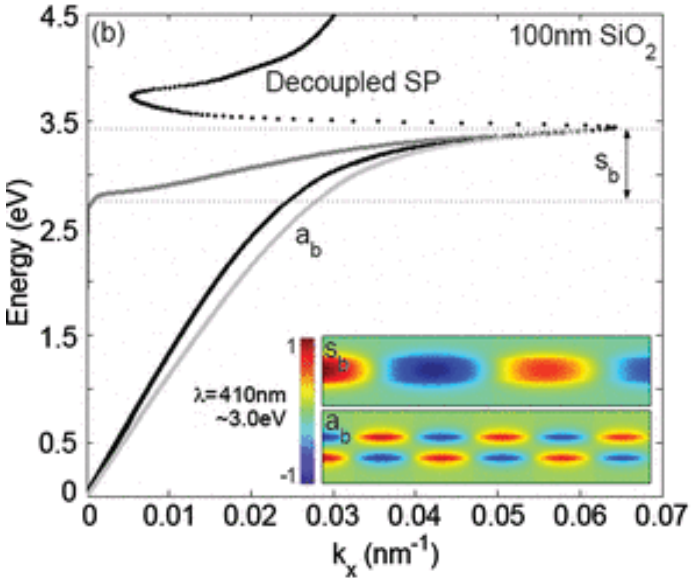

Figure 3: Simulation Result of Field Distribution in a Hybrid Plasmonic Waveguide [8, 9] Showing a Reduction in the K-Vector Compared to that in Free-Space and Effective Mode "Squeezing" in a Photonic Waveguide (top inset) vs Hybrid Plasmonic Waveguide (bottom)

High quality factor, Q resonant cavity photonic modulators suffer from bandwidth limitations and need to be optimized for a certain operating wavelength range [1,2]. In addition, resonant modulators are sensitive to temperature fluctuations and fabrication tolerances [1,2].

Plasmonic modulators, on the other hand, suffer from significant losses. Surface plasmons are nothing but charge density oscillations of the local electromagnetic field on a metal-dielectric interface stimulated by the electromagnetic field of incident photons. Charge-density fluctuations in a metal are nothing but moving electrons; moving electrons incur joule loss. This is the fundamental loss mechanism in all plasmonic devices and the trade-off for the extraordinary localization in such devices. A recently reported 29 μm plasmonic modulator had a loss of 12 dB corresponding to a loss of 4138 dB/cm [6].

A third approach, hybrid plasmonic modulators, have recently been reported [7,8] combining the advantages of photonic and plasmonic structures. Hybrid plasmonic waveguides (see Figure 4) consist of a thin noble metal layer, typically about 20 nm thick, sitting atop a thin layer of a nonlinear dielectric, which in turn sits on top of a traditional silicon photonic waveguide. The result is a structure wherein the photonic mode is "pulled" up from the Si waveguide by the noble metal and is located predominantly in the nonlinear dielectric layer between the Si and the noble metal. Critically, pulling a mode up from a photonic waveguide via a metal layer, rather than using a traditional metal-dielectric-metal plasmonic guiding structure, reduces the interaction area between the mode and the lossy metal while still retaining most of the plasmonic localization [7,8]. This serves to reduce losses to the order of 800–2,000 dB/cm while still supporting localized higher k-vector plasmonic modes. As a further advantage, the resulting mode sits almost entirely in the nonlinear material.

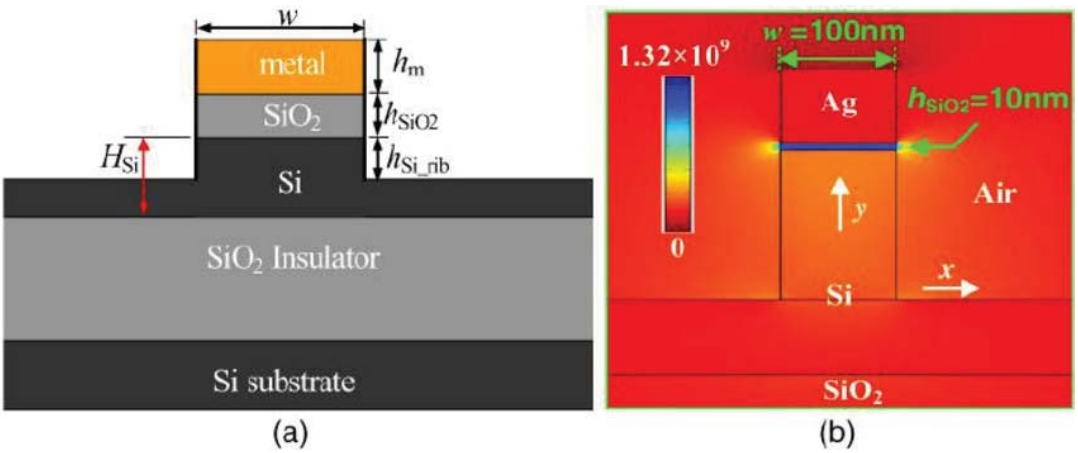

Figure 4: Illustrating Hybrid Plasmonic Waveguide [7]

These approaches all focus on realizing modulators in a waveguide configuration and are not suitable for the program goals of Defense Advanced Research Projects Agency (DARPA) MOABB effort. Nevertheless, these approaches form a useful jumping-off point as to the current state of the art and the techniques thereof. Constructing a 2D array of phase shifters to provide wide angular scanning (~120^0) with a high resolution (~0.5^o) will require ultra-compact phase shifters with footprint less than 1 μm^2 scalable to realize large 2D arrays with period on the order of 1 μm.

Our approach is to use hybrid plasmonic waveguides with a nonlinear material such as ZrO_2 in a vertical cylindrical topology coupling directly to free space (see Figure 2). These VCSEPs will realize a full 2π phase shift at a packing density $\geq 1/\mu m^2$. Specifically, arrays of VCSEPs will be fabricated on a wafer or chip and will be illuminated from below. When light passes through the VCSEPs it will be converted to a hybrid plasmonic mode where it will be localized and pass through a nonlinear material. Through combined localization and resonant effects, the interaction length will be greatly increased. A voltage will be applied to the metal shell via a metal contact (see Figure 2), and the doped Si core attached to a doped Si substrate will serve as the ground. This will induce an electric field within the nonlinear electro-optic material within the VCSEP, modulating the refractive index within an individual VCSEP pixel. The combination of greater effective interaction length and variable refractive index within the cavity will impart a phase shift to the light. The light will then be re-emitted into free space; in this configuration the VCSEP operates in transmission mode.

VCSEPs will use hybrid plasmonic localization to increase effective interaction length of light with nonlinear material within a resonant cavity. The increased interaction length, due to plasmonic effects in the vertical architecture, leads to greater phase shifts than those offered by other approaches. Lower loss (~1,000 dB/cm) is possible while retaining high localization (due to the overlap between the photonic and plasmonic modes). The impedance mismatch between the vertical hybrid plasmonic waveguide and free space will create a low finesse and low-Q cavity resonator.

By using a low-Q cavity we reduce the traditional limitations on bandwidth and spectral range found in high-Q resonator-based photonic modulators while still deriving a benefit from a longer interaction length due to a cavity finesse of 10-20. This effect also benefits from the large *k*-vector plasmonic modes that are localized in space: hybrid plasmonic modes stimulated by a free-space 1550 nm laser will have an effective wavelength that is up to 20x shorter in the hybrid plasmonic structure [8,9]. Combined with an example cavity finesse of 10 (i.e. assuming a photon will, on average, make 10 round trips through the cavity), the VCSEP will provide a 400x increase in effective interaction length with the nonlinear material. In other words, a 5-μm tall VCSEP may have an effective interaction length of 2000 μm or 2 mm with the nonlinear material.

The VCSEP will couple photonic modes to plasmonic modes through a lower index dielectric (e.g. SiNx, ZrO_2) [8,9] surrounding a high index core (e.g., Si) in the coaxial structure (see Figure 2). Taken together in a vertical topology, this hybridizes the advantages of plasmonic localization with a low-loss photonic mode, where metal also provides the electrical contact in an ultra-compact vertical topology (see Figure 2). Due to vertical architecture, the proposed VCSEP can have a very large packing density, $\geq 1/\mu m^2$. Flexibility in hybrid plasmonic design allows us to optimize for low loss (<1000 dB/cm) or high localization (e.g. $k_{mode} > 30k_{freespace}$), depending on the respective radii of the Si core, the interstitial layer of nonlinear dielectric, and the metal shell. With a small Si core, the photonic mode is forced into the nonlinear dielectric between the metal and the Si crating greater overall interaction with the nonlinear dielectric while retaining some plasmonic localization (Figure 5). With a thick Si core and thick metal cladding, the field is well confined in the nonlinear dielectric and strongly localized in a thin section of nonlinear dielectric at the expense of increased loss (Figure 5). This is a direct cylindrical analogue to the hybrid plasmonic waveguides typically found in the existing literature (see Figure 4).

Finite difference time domain (FDTD) simulations of Maxwell's Equations were performed using Lumerical. These FDTD mode simulations of the vertical cylindrical hybrid plasmon cavity [10] (diameter 400 nm) shown in Figure 2 are summarized in Figure 5 and predict a propagation loss of 2,000 dB/cm, which is consistent with values seen in literature for other hybrid plasmonic structures.

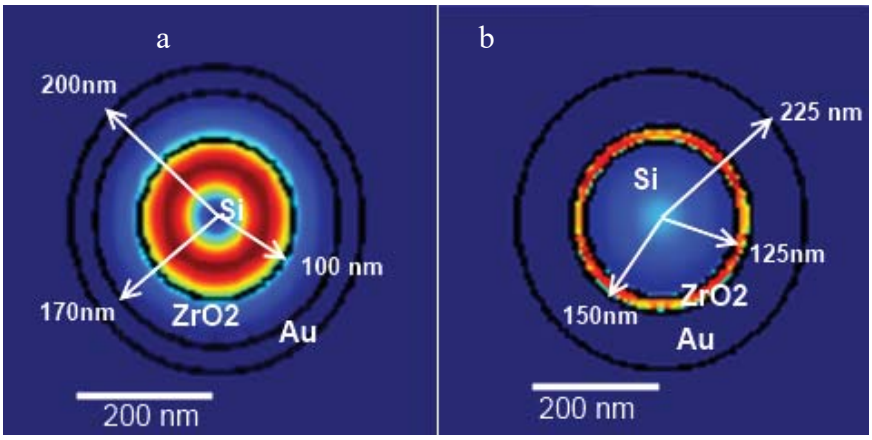

Figure 5: Description of Different Potential Configurations for the VCSEP and Corresponding Electric-Field Localization

As the radius of the Si core approaches the inner radius of the metal shell, the mode becomes increasingly localized in the ZrO_2 nonlinear dielectric. The geometry optimization enables control of the mode localized in the Si core, ZrO_2, and the metal shell, thereby allowing to optimize the loss and the nonlinear interactions.

In our example we assume a 5-μm long VCSEP structure with core Si pillar surrounded with ZrO_2 covered with metal (i.e., Si nanowires can be etched or grown to aspect ratios of 1:20). If we assume $\lambda_{eff\_hybrid\_plasmon} = \lambda_{free\_space} / 20$, then our hybrid plasmon mode will see the VCSEP as being 5 μm / (1.550 μm /20) = 64 wavelengths long. The transmission electron microscope (TEM) mode of the hybrid plasmonic VCSEP has an effective refractive index of 18.1. It is possible to estimate the finesse of the cavity using the following expressions:

$$F = \frac{e^{-\alpha_{tot}\, d/2}}{1 - e^{-\alpha_{tot}\, d}}$$

The total optical loss α_{tot} is expressed as:

$$\alpha_{tot} = \alpha_{int} + \frac{1}{2\,d}\ln\left(\frac{1}{R_1}\frac{1}{R_2}\right)$$

Where α_{int} ~ 1,000 dB cm^{-1} is the contribution of the metal loss and the last term of α_{tot} corresponds to contribution of the mirrors. For a cavity height of d=5 μm, the total loss is α_{tot} ~3,310 dB cm^{-1} corresponding to F~ 8.

On average, our photons will pass through ~450 $\lambda_{eff\_hybrid\_plasmon}$ in ZrO_2. Then the electrically induced $\Delta n = 0.00104$ due to the Kerr effect in the ZrO_2 layer will induce a phase shift of $\Delta\varphi = \pi$. Provided the Si nanowires can be fabricated with an aspect ratio of 1:20, we estimate that for a 0.5 μm diameter a length of 10 μm is feasible. With such geometry, the required $\Delta n = 0.00052$. For such a device, we estimate a Joules insertion loss of about 1 decibel (dB). The phase shift for different aspect ratio is summarized in Table 1.

Table 1. Estimated Phase Shift vs Aspect Ratio of VCSEP Device

Aspect Ratio	1:13	1:25	1:37
Phase Shift	π	~1.7 π	2 π

Using Si nanowires as a base and leveraging past experience in the design and modeling, fabrication and characterization of similar vertical cavity photonic resonators will allow us to fabricate large arrays of phase modulators/shifters using proven fabrication techniques as depicted in Figure 6.

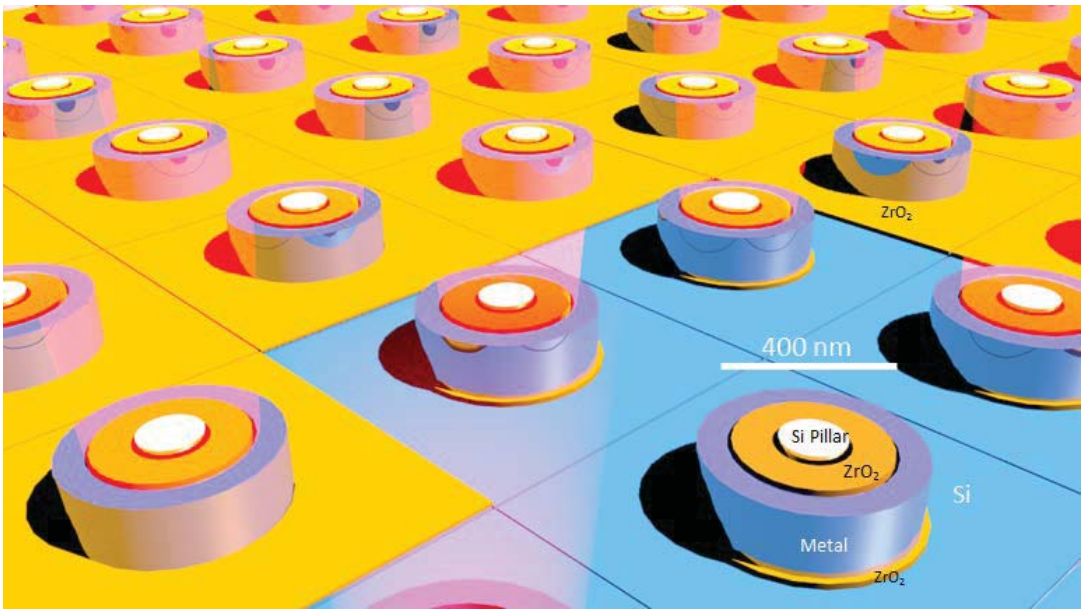

Figure 6: Illustration of the Proposed VCSEP Array

2.3 Scope

The scope of this project included investigating the compact phase shifting approach using quadratic electro-optic effect in a VCSEP. The study explored:

1. A hybrid plasmonic micro-patch three dimensional (3D) resonator on a μm-scale which enables x20 times reduction of the effective wavelength resulting in a < 1 μm^2 footprint device,
2. The quadratic electro-optic and other electro-optic effects to enable ultrafast operation at low voltages supporting operation at 5 μW/(2π) and
3. A 2D array of VCSEPs with a period of 1 μm.

The developments produced by this effort are applicable to beam forming/scanning in a wide angular range (~120^0) with high resolution (~0.5^o) and may contribute to the development of an enabling MOABB technology. The tasks undertaken represented different technical approaches, initially pursued in parallel to diversify risk, and subject to down-selection later in the program. The originally proposed VCSEP Metrics and Milestones are summarized in Table 2.

Table 2. Program Metrics and Milestones

	Phase I (9 mo.)	Phase II (9 mo.)
Power	10 μW/2π	5 μW/2π
Footprint	~1 μm^2	< 1 μm^2
Insertion loss	< 6 dB	< 2 dB
Response time	~ 1 μsec	~ 1 nsec
Operating temperature	room	100°C
Operating wavelength bandwidth	>10 nm	>30 nm
Array size and interference	-	8x8

Power:
The power requirements for an individual VCSEP can be calculated as follows: $W=1/2\ V^2/\Omega$ where W is the required power to flip a bit, V is the applied voltage to the metal shell, and Ω is the impedance of the shell. $|\Omega| \approx R/C$, where C is the capacitance of the VCSEP and the resistance R comes from the ZrO_2 resistance between the shell (contact) and Si pillar (ground). For our cylindrical topology, the capacitance is given by $C = L\times 2\pi\times\varepsilon_r\times\varepsilon_0/\ln(b/a)$, where L is the length (or height) of the cylinder, ε_r is the relative permittivity of the dielectric, ε_0 is the permittivity of free space, a is the radius of the cylindrical capacitor (the radius of the Si core, the ground contact in our case), and b is the inner radius of the metal shell. In this work, we take $L = 5\mu m$, $\varepsilon_r = 0.5\times10^{-6}$ F/m, $\varepsilon_0=8.8\times10^{-12}$ F/m, b= 0.17 μm, and a=0.10 μm. This gives us $C = 2.6050\times10^{-19}$ F. We know R from the material characteristics of ZrO_2 and the dimensions of the ZrO_2 layer in our device, $R=3.16\times10^5$ Ohm/m$\times0.07\times10^{-6}$m = 0.0221 Ohm. This gives an impedance $|\Omega|=0.0221$ Ohm $/2.6050\times10^{-19}$ F = 8.4837×10^{16} Ohm/F. Assuming our Table 2 target of using 5 μW of power to impart a 2π phase shift to the light in our device, and assuming we modulate the individual pixels at 1 Gb/s (or a period of 1 ns at 5 μW corresponding to 500 fJ per bit) we can estimate the necessary Voltage or $V_{2\pi}$ as follows: $W=1/2\ V^2/\Omega$ 5 μW ×1 nsec = ½ $\times8.4837\times10^{-16}$ F × V^2. Solving for the required voltage V yields $V_{2\pi}$ = 3.43 Volts at 500 fJ/bit.

Footprint:
The construction of a 2D array of phase shifters in support of MOABB requires the construction of ultra-compact phase shifters with footprints less than 1 μm^2 scalable to realize large 2D arrays with periods on the order of the operating wavelength to achieve the steepest deflection angle (e.g., +/- 60^0). For operation in the telecommunication wavelength it will correspond to a period of 1.5 μm or less. This requires that the footprint of each phase shifter in the array is ~ 1 μm^2. To achieve a ~0.5° resolution, we need to assure scalability to be able to construct a large device aperture (i.e., arrays > 240×240 elements).

Insertion loss:
The insertion loss metric of the VCSEP is introduced to account for loss due to the absorption by the metal and the loss due to the use of a resonant structure. By varying the geometric design parameters of VCSEP, and through a careful choice of material composition, the insertion loss can be minimized to meet the metric needed by the applications.

Response time:
The response time metric of the VCSEP device depends on the time response of the nonlinear optical material inside the resonator, the resistance, and the capacitance of the VCSEP device. We intend to include the time response characteristic into the proposed VCSEP architectures studies and consider it during the down selection process of the architectures for experimental realization and characterization.

Operating temperature range:
The operating temperature metric is introduced to assure that the VCSEP device can operate with a narrow band optical frequency source in a broad range of temperature variations. Since the proposed device is resonant, temperature variations will cause a shift in the resonant transmission bandwidth and thus affect device operation. We will investigate the temperature dependence of the various VCSEP device architectures and designs and determine strategies for robust operation of the device (e.g., electronic adjustment of phase distributions, heat extraction via metal layer, temperature stabilization). The thermal management of the device will be investigated using full thermal simulations.

Operating wavelength bandwidth:
The operating wavelength bandwidth metric will depend on the VCSEP device architecture with its corresponding design (finesse of the resonator, shift of the center of the transmission band vs temperature, etc.). We will investigate the wavelength bandwidth dependence of various VCSEP designs and determine strategies for robust operation of the device in a broad spectral range exploiting athermal design approaches, thermal management, as well as active stabilization.

Array size and interference:
The array size metric is introduced to quantify the scalability of the proposed VCSEP approach to meet the needs of the beam forming applications with high angular resolution. The size of the array (i.e., aperture) determines the far field resolution or the diffraction limited minimal size of the formed optical field. Therefore, the small size (i.e., the period) of about a μm in our current VCSEP device design goals will be able to support arrays on the order of 10000×10000. However, we introduce this metric with main objective to quantify possible interference between adjacent devices in the array. This parameter will be quantified during the modeling various VCSEP architectures/designs and experimental validation in a small size arrays.

2.4 Risk Assessment

The proposed phase-shifter design has no equivalent in the literature, and may face technical challenges. These are mitigated by the diversification of different architectures approaches along with the identification of the optimal materials. The proposed research plan sought to address the technical risks enumerated and discussed next.

Total loss:
The total loss governs the number of transit of the coupled beam into the cavity, which plays an important role in the phase-shifter performance. We identified two main sources of loss: the materials absorption and interface reflectivity. The materials, which inherently induce optical losses, are the metal cladding, the interstitial dielectric, and the silicon core. The total loss will be mitigated by optimizing the cavity architecture with a careful choice of a

low-loss interstitial dielectric while maximizing the phase-shift. We therefore mitigate this risk by a careful design of the cavity as well as a characterization of the different candidate materials (ZrO_2, dielectric-aSi-dielectric, High Si SiNx and BTO).

Thermal effects:
Heating may affect the cavity resonance wavelength. Assuming a thermo-optic coefficient for refractive index of Si, $2x10^{-4}\ ^oC^{-1}$, we estimate a shift of the resonance by about $10^{-5}\ \lambda/^oC$. The contribution from the Si is small, however the proposed cavity architecture is more complex as it is based on multilayer materials with a cylindrical geometry on top of a planar substrate. Thus, the thermal management of the device will be investigated using full thermal simulations.

Capacitor and leakage current:
The VCSEP utilizes the capacitance effect to induce an electric field across the interstitial dielectric. Our analysis discussed in Sec. II.A, provides an order-of-magnitude estimate of the capacitance assuming a uniform electric field. Because of the complexity of the phase-shifter geometry, the electric field distribution with respect of the interstitial material is an important feature to address and understand. In this regard, detailed numerical simulations will be performed. Another feature that requires careful attention as it may affect the performance of the phase-shifter is the leakage current through the interstitial dielectric. This effect may drop the energy needed to operate the device. These two technical risks will be investigated and then taken into account during the design process.

3. METHODS, ASSUMPTIONS, AND PROCEDURES

3.1 Task 1 Design of VCSEP Resonator

The first task of this program will address the following objectives:

- Investigate and optimize VCSEP architectures to meet the requirements noted in Table 2. Produce numerical estimates of hybrid-plasmon open-mode resonators with respect to loss, finesse, and coupling characteristics.
- Down-select specific hybrid-plasmonic open-mode resonators with optimal characteristics in terms of the proposed metrics.
- Design/evaluate our selection of electro-optic material for phase shifting using such materials as ZrO_2, dielectric-aSi-dielectric, high Si SiNx, and BTO.
- Design of the electrical contacts to Si (ohmic) and Al.
- Optimization of the VCSEP design tolerant to temperature and broadband operation.
- Design of a scaled-down array of VCSEP phase shifters with variable period to estimate electrical and optical isolation and independent control capabilities

Each of objectives relies on the following approaches:

- Define various architectures of the VCSEP device considering the interface with the optical input circuits.
- Identify material composition for realization of these architectures.
- Use various simulation and modeling tools (COMSOL, Silvaco, Lumerical) to conduct metaphysics analysis.
- Establish quantitative analysis to estimate the defined metrics.

3.2 Task 2 Fabrication of VCSEP device

The aim of the Task 2 will be devoted to achieving the following objectives:

- Develop fabrication methods of electro-optic material for phase shifting
- Develop fabrication procedure of VCSEP resonator using Si nanowire clad with ZrO_2 and Al for passive characterization
- Develop fabrication procedure of VCSEP resonator using Si nanowire clad with ZrO_2 and Al for active characterization
- Develop a fabrication procedure of electrical contacts
- Develop a fabrication procedure for wire bonding to electrical contacts
- Develop a fabrication process to demonstrate a scaled-down array of VCSEPs

Our fabrication approach is based on the following:

- The use of spattering and atomic layer deposition (ALD) methods for the fabrication of electro-optic materials
- Leveraging a silicon-on-insulator (SOI) material platform for the fabrication of Si wire arrays exploiting etching and growth approaches.
- Investigate various metal deposition methods to construct ohmic contacts to Si and Al

3.3 Task 3 Characterization of VCSEP device

- The last task is aimed to achieve the following objectives: Evaluation of electro-optic materials for phase shifting followed by a down selection of the most attractive VCSEP device.
- Measurement of the static parameters of the VCSEP passive resonators (e.g., total loss, tolerance to temperature and wavelength) and use this data for design of active device.
- Evaluation of the electrical contacts to VCSEP device for high-bandwidth operation providing feedback for task 1.
- Testing the VCSEP phase shifter vs operating frequency to meet the proposed metrics
- Develop characterization methods of a scaled-down array of VCSEP phase shifters to determine electrical and optical isolation vs period.

Approach:

- Use the z-scan technique to characterize the nonlinear properties of electro-optic materials for phase shifting.
- Develop ohmic contacts characterization setups.
- Use spectral characterization setup to determine spectral response of the VCSEP device.
- Utilization of the interferometry techniques for measuring phase shifts of VCSEP device.
- Utilization of free-space optical Fourier transform techniques for characterizing the VCSEP array.

4. RESULTS AND DISCUSSION

In this section, we present the detailed results and discuss each of the tasks above. Section 4.1 explains the obtained results during the instigation and optimization of the VCSEP architecture. Section 4.2 discusses the design and fabrication of the VCSEP phase shifters. Section 4.3 explains the characterization process of the obtained devices. The final section discusses the obtained results from the characterization of a single VCSEP.

4.1 Optimization of the VCSEP Architectures

Lumerical FDTD simulations led to two attractive VCSEP designs which we sought to fabricate. A lower loss (~1300 dB/cm) configuration [see Figure 7(a)] where the hybrid photonic/plasmonic mode is moderately localized by the Aluminum shell, but primarily serves to pull the photonic mode out of the high index Si core into the EO dielectric layer.

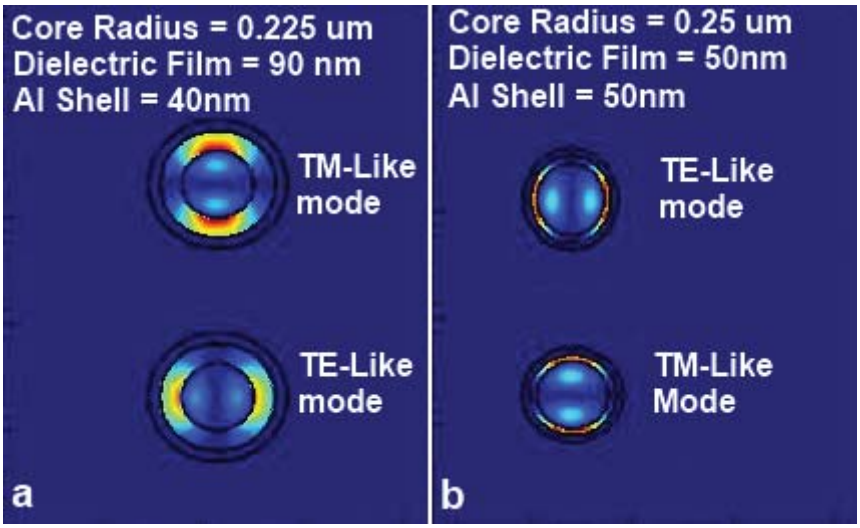

Figure 7: FDTD Simulation for VCSEP Architectures with Varying Parameters

This configuration is optimized for the high r_{33} polymer as described below, as it leverages an extremely good mode overlap between the EO material and the photonic mode. A second configuration [Shown in Figure 7b] relies on greater plasmonic localization but comes with a higher loss of ~2300 dB/cm. This configuration has higher plasmonic localization for use with a material platform with a weaker overall electro-optic effect.

4.2 Design & Fabrication of a Scaled-down Array of VCSEP Phase Shifters with Variable Period

We designed and fabricated a scaled down array of VCSEPs to validate our developed fabrication procedures and steps with fabrication results presented in Figure 8.

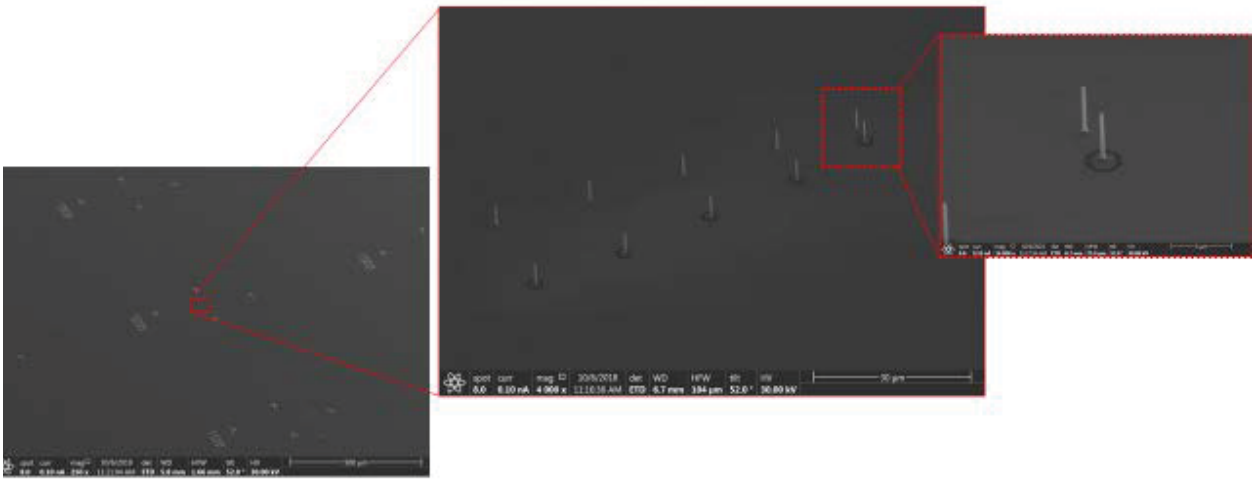

Figure 8: SEM Micrograph Illustrates a Fabricated Scaled-Down Array of VCSEP Phase Shifters with Variable Spacing

Scaled-down arrays of VCSEP phase shifters with variable period were fabricated as per our Task 1 specification to characterize the independence and optical isolation of nearby VCSEPs. It is necessary to establish that (1) light from nearby VCSEPs is coherent and (2) that the adjacent VCSEPs may be independently controlled i.e. optical output can be phase shifted electrically with respect to one another. The subsequent experiments characterizing VCSEP interference fringes are designed to demonstrate (1) and (2) while offering some initial characterization of principal figures of merit. Specific device design for characterization of these properties are shown in Figure 9.

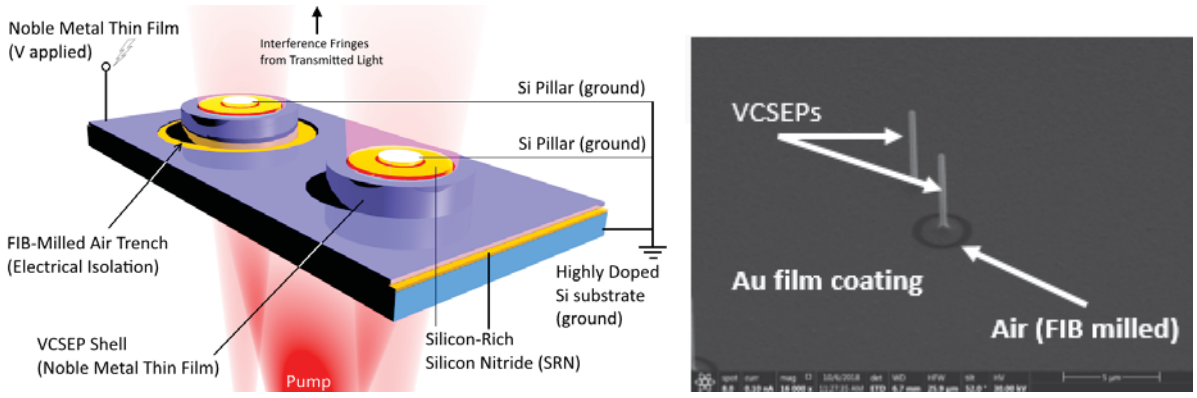

Figure 9: Illustration of VCSEP Configuration for Quasi-DC Characterization and SEM of the Fabricated VCSEP Device

In order to quantify the phase shift induced by our VCSEP, we perform an interferometric measurement of the fringes produced by two adjacent VCSEPs. By applying a voltage to just one of these VCSEPs and keeping the other as a reference, we will induce phase shift (δ) that will shift the fringe pattern produced by interference. Note that we used a focused ion beam (FIB) to electrically isolate one of the VCSEP devices from the electrode, thus by applying an electric field only one of the two VCSEP devices will be actuated. Knowing the observed shift in fringes (Δy_m), along with the pitch of the VCSEPs, and the distance to the plane imaged in our measurement setup, we can extract the induced phase shift (δ). From the induced phase shift (δ), we can characterize the device in terms of $V_\pi L$, Δn_{eff}, etc.

4.3 Task 3: Characterization

In this section, the characterization steps are explain by dividing the tests into subsections to address the characterization system, the results, the process to create ohmic contacts to the Si wafer, the characterization of the nonlinear optical materials as well as characterization of a single VCSEP device.

4.3.1 Characterization of the VCSEP Device

For the characterization of our initial VCSEP devices shown in Figure 9, we constructed an interferometric set up similar to a double slit experiment as shown in Figure 10.

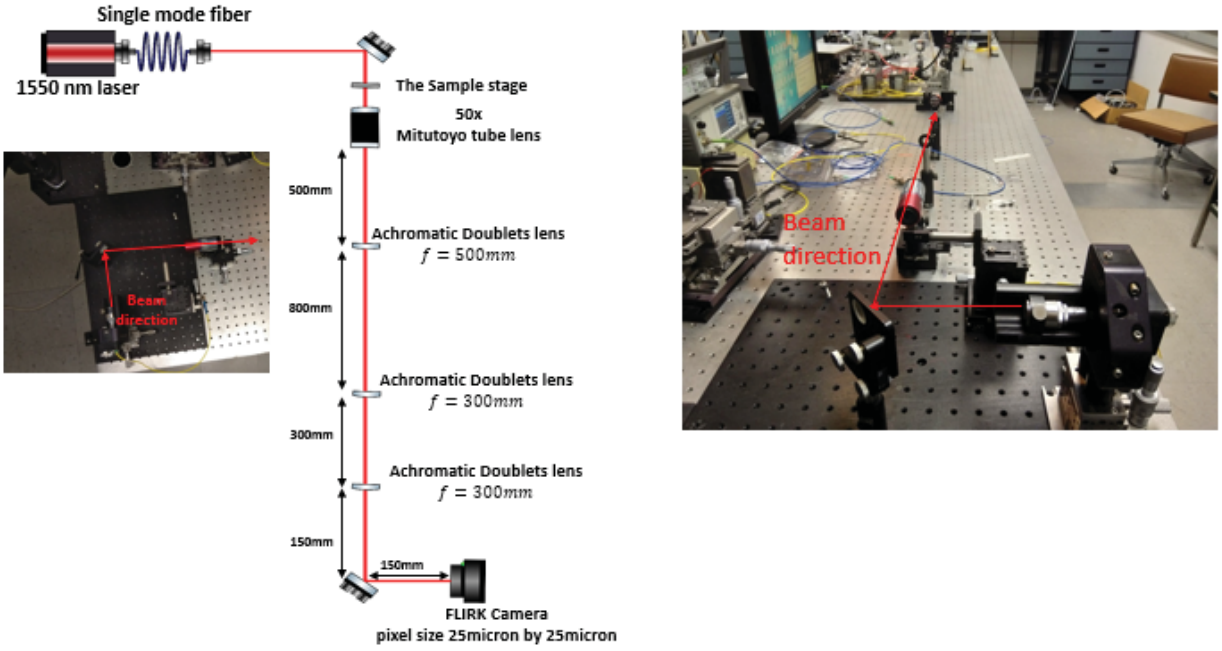

Figure 10: Schematic and Photograph of Optical Layout used for VCSEP Characterization

The un-modulated phase at point P in the far field from two identical, coherent sources is given by:

$$\Delta\varphi = 2\pi\frac{\Delta r}{\lambda} = 2\pi\frac{d}{\lambda}sin\theta$$

While the total electrical field form the two sources is given by:

$$E_p = 2E_0e^{-i\omega t}e^{ikr}\cos\left(\frac{\Delta\varphi}{2}\right)$$

The bright fringes from the un-modulated interference of these two VCSEP sources will occur when

$$\Delta r = m\lambda \text{ , at: } \theta_m = \frac{m\lambda}{d} \text{ , } y_m = \frac{m\lambda L}{d} = \frac{\Delta r L}{d} = \frac{\lambda\Delta\varphi}{2\pi}\frac{L}{d}$$

Introducing phase modulation by applying a voltage across one of the two VCSEPs,

$$\Delta\varphi \rightarrow \Delta\varphi + \delta$$

the field and intensity distributions become:

$$E_p = 2E_0e^{-i\omega t}e^{ikr}\cos\left(\frac{\Delta\varphi+\delta}{2}\right) \text{ and } I_p = 4I_0\cos 2\left(\pi\frac{d}{\lambda}sin\theta + \frac{\delta}{2}\right)$$

The corresponding shift in the location of the fringes, Δy_m is then given by:

$$\Delta y_m = \frac{\lambda\delta}{2\pi}\frac{L}{d}, \text{ solving for } \delta \text{ yields: } \delta = \frac{d}{L}\frac{2\pi}{\lambda}\Delta y_m$$

Here d is the spacing between VCSEPs, L is the path length between the plane being imaged and the FLIR sc2600 IR camera used to visualize the near field, λ is 1,550 nm, and Δy is the measured shift in interference fringes (see Figure 11).

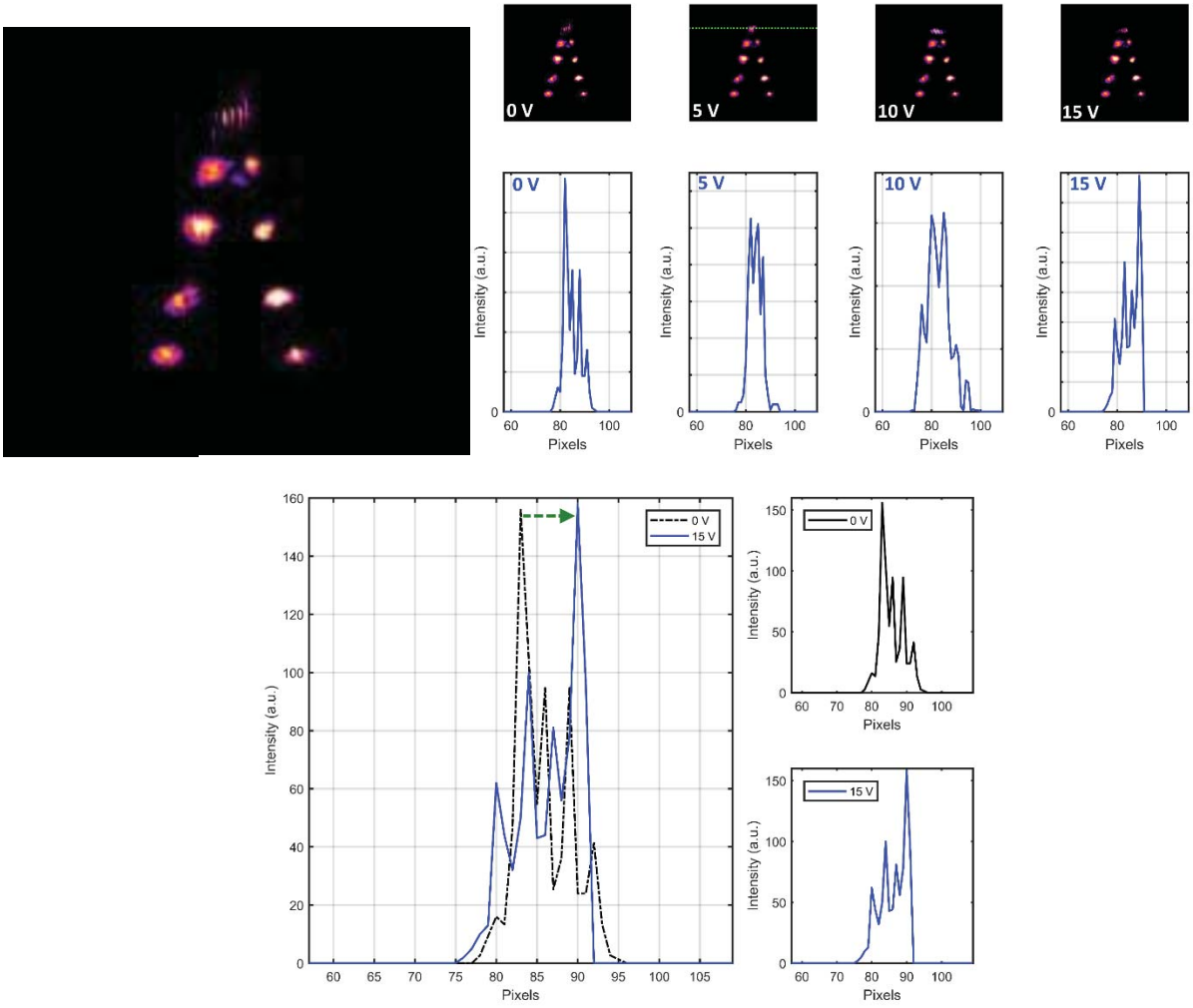

Figure 11: Initial Characterization of VCSEP via Described Fringe-Shift Method

Fringe shifting is observed near the image plane as a function of voltage for two VCSEPs at a separation of 2 μm under quasi-DC operation (see Figure 11). Measuring the intensity cross-section of the fringe pattern at varying applied voltages, it is possible to estimate an approximate phase shift (δ) to the applied voltage to one of the VCSEPs using equation

$$\delta = \frac{d}{L}\frac{2\pi}{\lambda}\Delta y.$$

Here, Δy is measured from the camera image, its pixel size, and using the magnification factor of the microscope used to image the VCSEPs. Additionally, using other known parameters such as d, L, and λ we can extract δ. The measured results are summarized in Table 3.

Table 3. VCSEP Parameters Extracted from Initial Proof-of-Concept Demonstration

	δ	$V_\pi L$	Δn_{eff}	height	aspect ratio	pitch
VCSEP gen_1	1.33π rad	0.0038 V-cm	0.3	3.35 μm	8.3:1	2 μm

4.3.2 Characterization of the Electrical Contacts

Making good ohmic contact with silicon is essential to the VCSEP for both high frequency performance and reducing $V_{\pi}L$. To that end, transfer length method (TLM) measurements have been performed to optimize the annealing process for good quality ohmic contacts to highly doped silicon substrates. Figure 12 shows the mask we have constructed to fabricate samples and measure the sheet resistance of the ohmic contacts. The extracted sheet resistance (see details in Figure 12) are found to be sufficient for electrical characterization of VCSEP devices where the two electrodes are created between Si and the metal coating the VCSEP device.

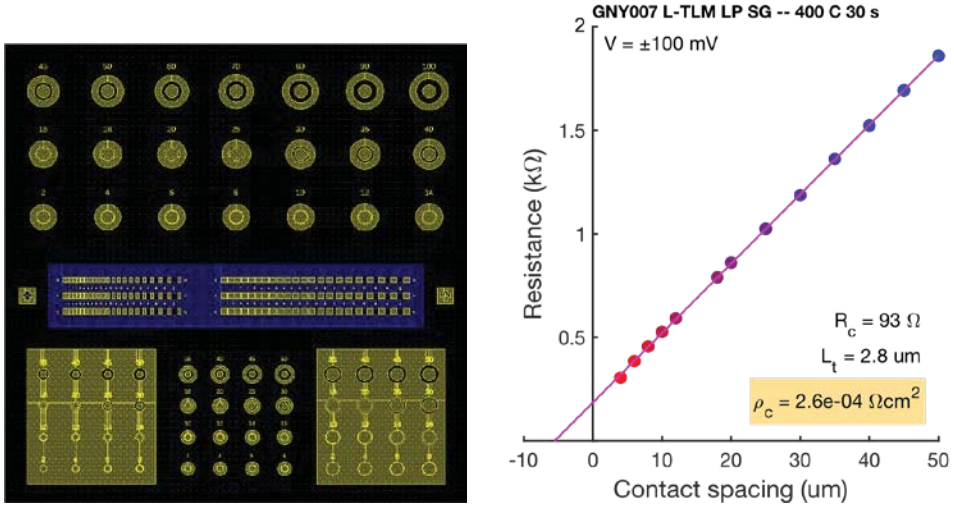

Figure 12: TLM Test Substrate and Contact to Si Wafer Resistivity Measurement

4.3.3 Nonlinear Optical Response Characterization of Si-rich SiN Films for VCSEPs

We investigated two materials as potential candidates for the electro-optic layer in the VCSEP device. The first one was via ALD of TiO2. This approach should exploit the dc-induced Pockels effect due to the high $\chi^{(3)}$ nonlinearity present in TiO2. The second approach was to use a silicon-rich silicon nitride (SRN) film deposited using a novel fabrication process in plasma-enhanced chemical vapor deposition (PECVD). In the literature, it has been shown that as the ratio of silicon to nitride in SRN increases, so too does its $\chi^{(3)}$ coefficient. The highest range of tunability reported via second-harmonic generation (Figure 13) in the SRN thin film with refractive index of 2.25 corresponds to an effective measured $\chi^{(2)}$ of 22.7 pm/V. We point out that we are now investigating ultra-rich SRN (USRN) films with refractive index of 3.2 and expect to increase the effective $\chi^{(2)}$ coefficient to values ~200 pm/V.

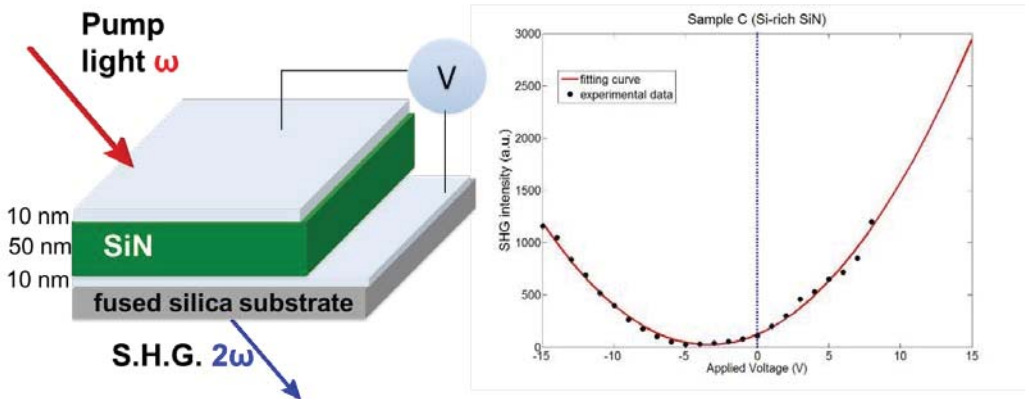

Figure 13: Illustration of Second Harmonic Generation via EFISH Process in Silicon Nitride to Estimate the Effective Second-Order Nonlinear Response

We have continued our investigation of various CMOS compatible materials for electro-optics applications. Figure 14 provides a summary of the effective $\chi^{(2)}$ coefficient that can be obtained at electric fields close to but still below the break down voltage.

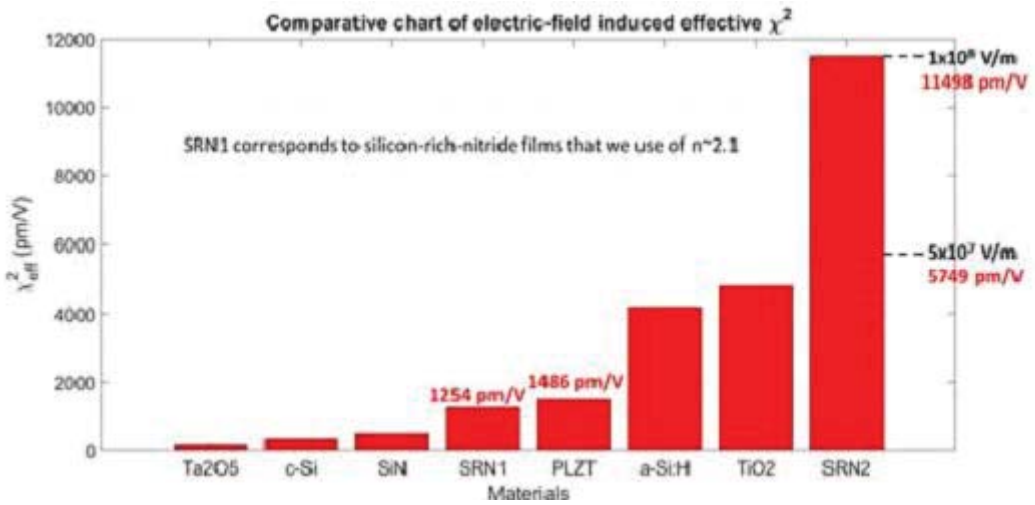

Figure 14: Effective χ(2) Nonlinearities in Various Thin Film Platforms at High Externally Applied DC Electric Fields

More recently we conducted a rigorous study of USRN in a waveguide configuration to investigate the DC-induced Pockels effect for fast modulation. To carry out this work we designed a racetrack resonator with a reasonably high Q-factor, 13,944 and 14,651 for the transverse electric (TE) and transverse magnetic (TM) like polarizations, respectively (see Figure 15a). We used a 250-µm straight section in a point-coupled configuration (see Figure 15b). Our device architecture is based on a 320-nm thick PECVD deposited SRN device layer on top of a 3 µm wet thermal oxide on Silicon. This 320-nm thick SRN layer is then dry etched using reactive ion etching in an Oxford P100 etcher using a 500-nm thick fox-16 soft mask written by electron beam lithography. The etched devices are then top clad by a 1-µm thick PECVD SiO_2 layer. Electrode traces 30-µm wide with a 10-µm separation are then patterned on top of the top clad, using an AZ1512/SF9 soft mask and DC sputtering of gold in a

Denton 635 sputtering system (see the design in Figure 15c and the field distribution in Figure 15d).

Figure 15d shows that by choosing the electrode trace width and spacing the applied field distribution can be made to create a difference in the in-plane versus out-of-plane applied fields as large as three orders of magnitude.

This allows us to uniquely attribute electro-optic measurements of the TE- and TM- polarized optical modes to tensor components $\chi 1331^{(3)}$ and $\chi 3333^{(3)}$ respectively. For characterization purposes, we used a combination of optical and electro-optic measurements to fully extract the material parameters of interest and in doing so demonstrate electro-optic switching based on the quadratic electro-optic effect.

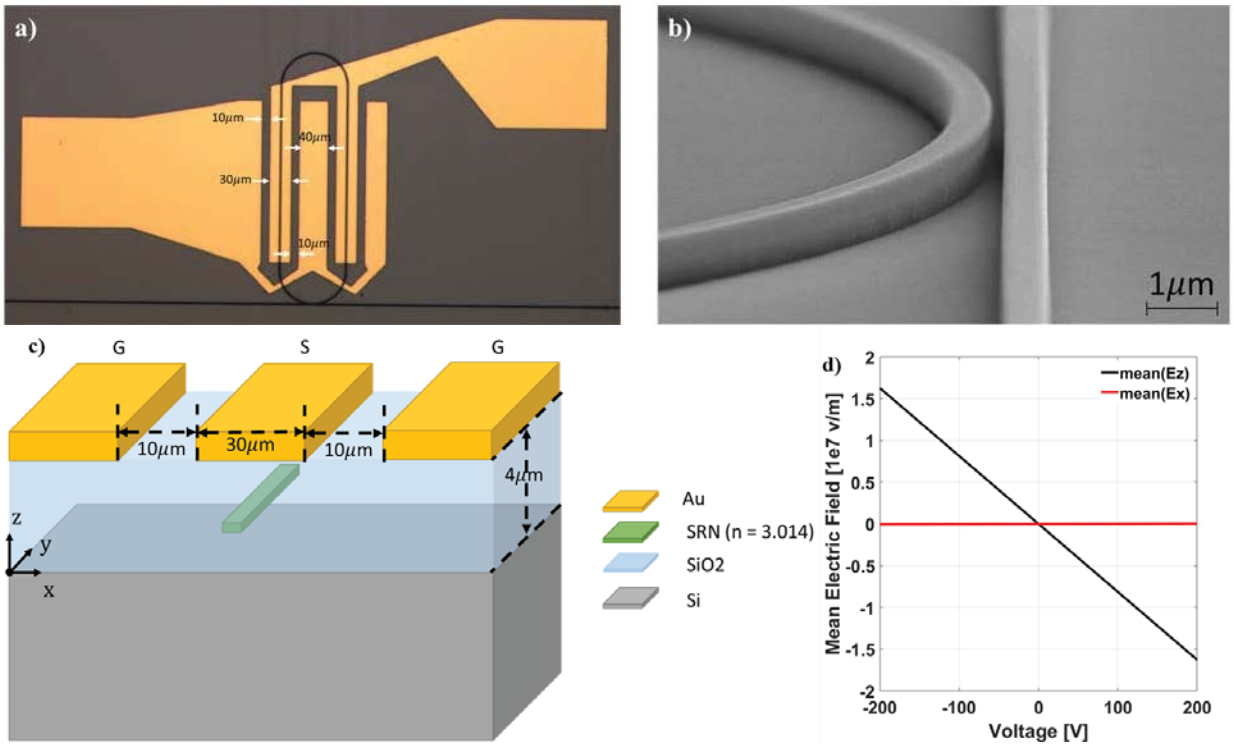

Figure 15: (a) Optical Microscope Image of our Point Coupled Micro-Ring Resonator with Electrode Width and Spacing Marked with White Arrows and Text Overlay, (b) Scanning Electron Microscope Image of the Point Coupler Region, (c) Schematic Breakdown of the Phase Shifter Design Shown as a Cutout, and (d) Plot of the Mean Value of the Applied Field Ex and Ez Components vs Voltage inside the Waveguide Core

Figures 16(a) – (d) and Figures 16(e) – (h) show the measured results for the TE- and TM- polarizations, respectively. We achieved a maximum extinction ratio of ~16dB and ~13dB for the TE and TM cases, respectively. The corresponding change in the effective refractive index can be seen in Figures 16(c) and (g) and by design we can extract one of the two contributing unique third-order nonlinear susceptibility tensor components, $\chi 1331^{(3)}$ and $\chi 3333^{(3)}$ for TE and TM modes, respectively.

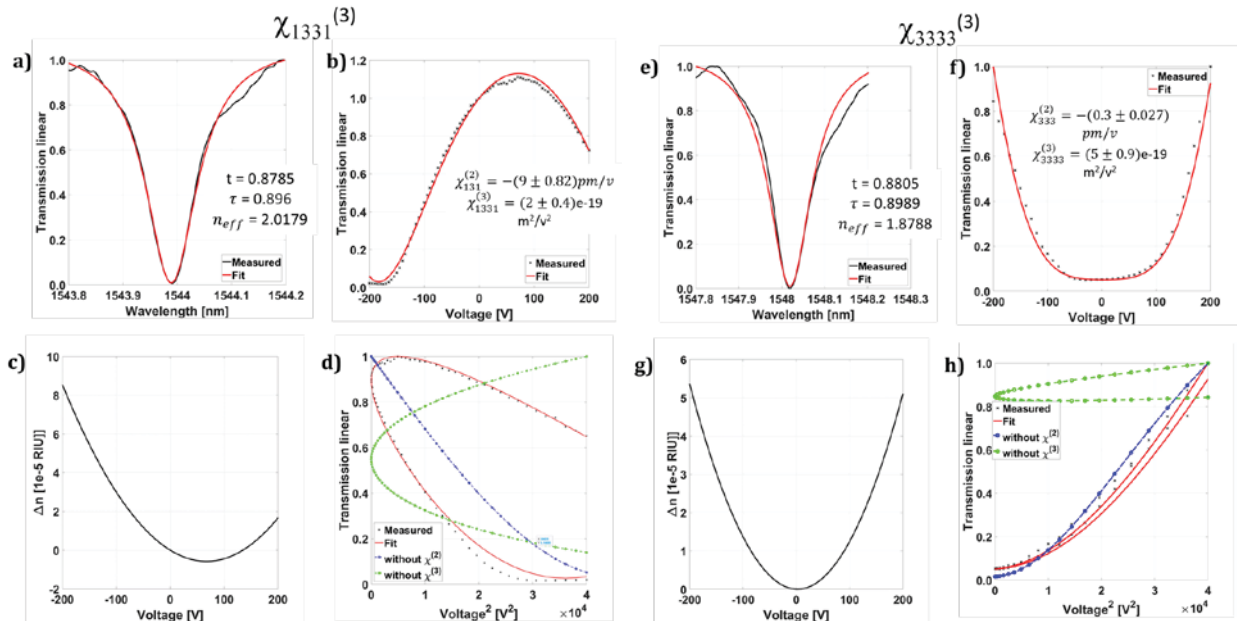

Figure 16: (a)-(d), (e)-(h) Measurements of Transmission vs Wavelength and Transmission vs Applied Voltage for the Case of the TE- and TM- Polarized Optical Modes Respectively
(a) Plot of transmission versus wavelength for one resonance of TE- polarized optical mode. (b) Plot of transmission versus applied voltage operating at a fixed wavelength of 1544.02 nm in the TE- polarized optical mode case normalized to the transmission at 0 volts applied. (c) Plot of the extracted change in effective refractive index versus applied voltage for the TE case. (d) Plot of transmission versus applied voltage squared at a fixed wavelength of 1544.02 nm in the TE- polarized optical mode case normalized to the maximum transmission. (e) Plot of transmission versus wavelength for one resonance of the TM- polarized optical mode. (f) Plot of transmission versus applied voltage operating at a fixed wavelength of 1548.02 nm in the TM- polarized optical mode case normalized to the maximum transmission. (g) Plot of change in effective refractive index versus applied voltage for the TM case extracted from (f). (h) Plot of transmission versus applied voltage squared at a fixed wavelength of 1548.02 nm in the TM- polarized optical mode case normalized to the maximum transmission. Effective χ(2) nonlinearities in various thin-film platforms at high externally applied DC electric fields.

Two measurements are performed in our experimental characterization: we first measured the passive transmission spectra of our racetrack resonators, followed by a second measurement of the transmission spectra as a function of the applied voltage at a fixed wavelength. These two measurements are repeated for TE- and TM- polarizations.

Figures 16(d) and 16(h) show the active optical results versus applied voltage squared for TE- and TM- respectively. If a film was purely $\chi^{(2)}$ then it should exhibit odd symmetry while a purely $\chi^{(3)}$ film should exhibit even symmetry. This means that in the general case of a film exhibiting both $\chi^{(2)}$ and $\chi^{(3)}$ plotted in this manner the film should have a symmetry around an axis which is rotated based on their relative contributions.

In summary, we demonstrated that a low-loss PECVD SRN film with a refractive index of 3.0 or higher can be used for electrical switching with an extinction ratio of ~16dB and ~13dB in TE and TM modes respectively. By optimization of the electrode design significant reductions to required voltages can be achieved. Furthermore, we demonstrate that these films still exhibit a breakdown field as large as 1.2E8 V/m and exhibit an RF permittivity of 9.06. Therefore, electro-optic switching in SRN using the quadratic electro-optic effect is clearly a viable path forward and deserves further exploration. This work also highlighted that SRN is a very promising material platform with desirable properties for a variety of on-chip applications beyond that of wave mixing.

4.3.4 Characterization of a Single VCSEP Resonator

Characterization of a single VCSEP device is challenging mostly because the whole device is only about ~1 μm in diameter. Therefore we had to rebuild our characterization setup to enable high-resolution imaging to "find" the single VCSEP device under test as well as design and fabricate new samples that incorporated larger size alignment marks that identify the smaller area where a single VCSEP or a pair of VCSEPs are located in the fabricated structure. Scanning electron microscope (SEM) and optical images of such a fabricated structure are shown in Figure 17.

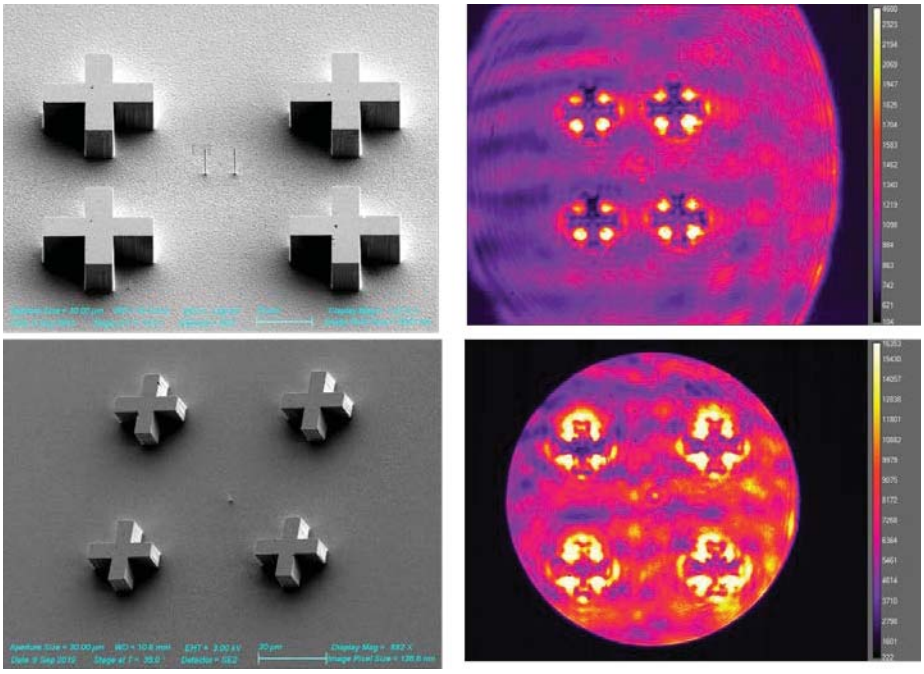

Figure 17: SEM Image of the VCSEP Devices (left) with the Larger Size Alignment Marks for its Identification in Optical Microscope and Optical Image of the Structure Obtained using a FLIR Camera with Illumination using a 1550-nm Laser (right)

The schematic diagram of our constructed optical system for characterization of single VCSEP device is shown in Figure 18.

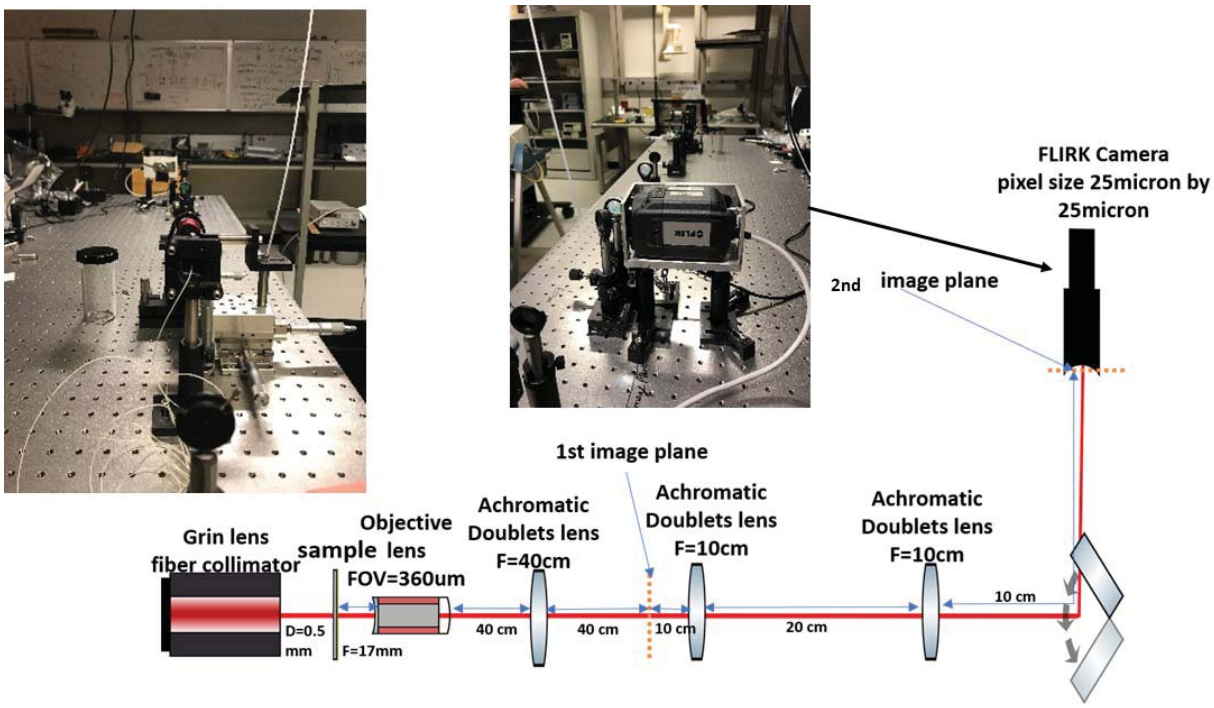

Figure 18: Schematic Diagram of the Microscope System Designed and Constructed for Characterization of a Single VCSEP Device

The optical images of the constructed characterization system are also included.

With the alignment marks, we were able to identify the location of a single VCSEP device and were subsequently able to obtain transmission of light coupled into a single VCSEP device as shown in Figure 19.

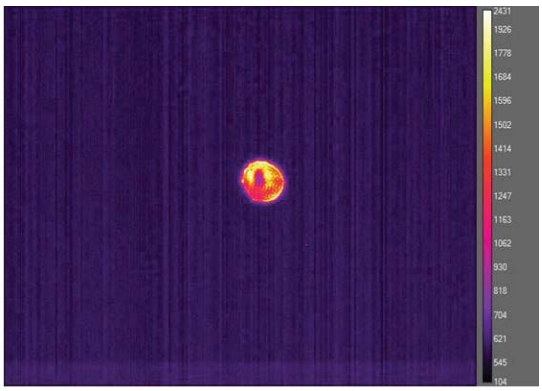

Figure 19: Optical Image Detected by the IR Camera Showing Transmission of Optical Field through the Single VCSEP Device

We next performed the optical characterization of the single VCSEP device using a tunable laser using a tuning range of 1460 nm to 1640 nm. The measured transmission results are summarized in Figure 20.

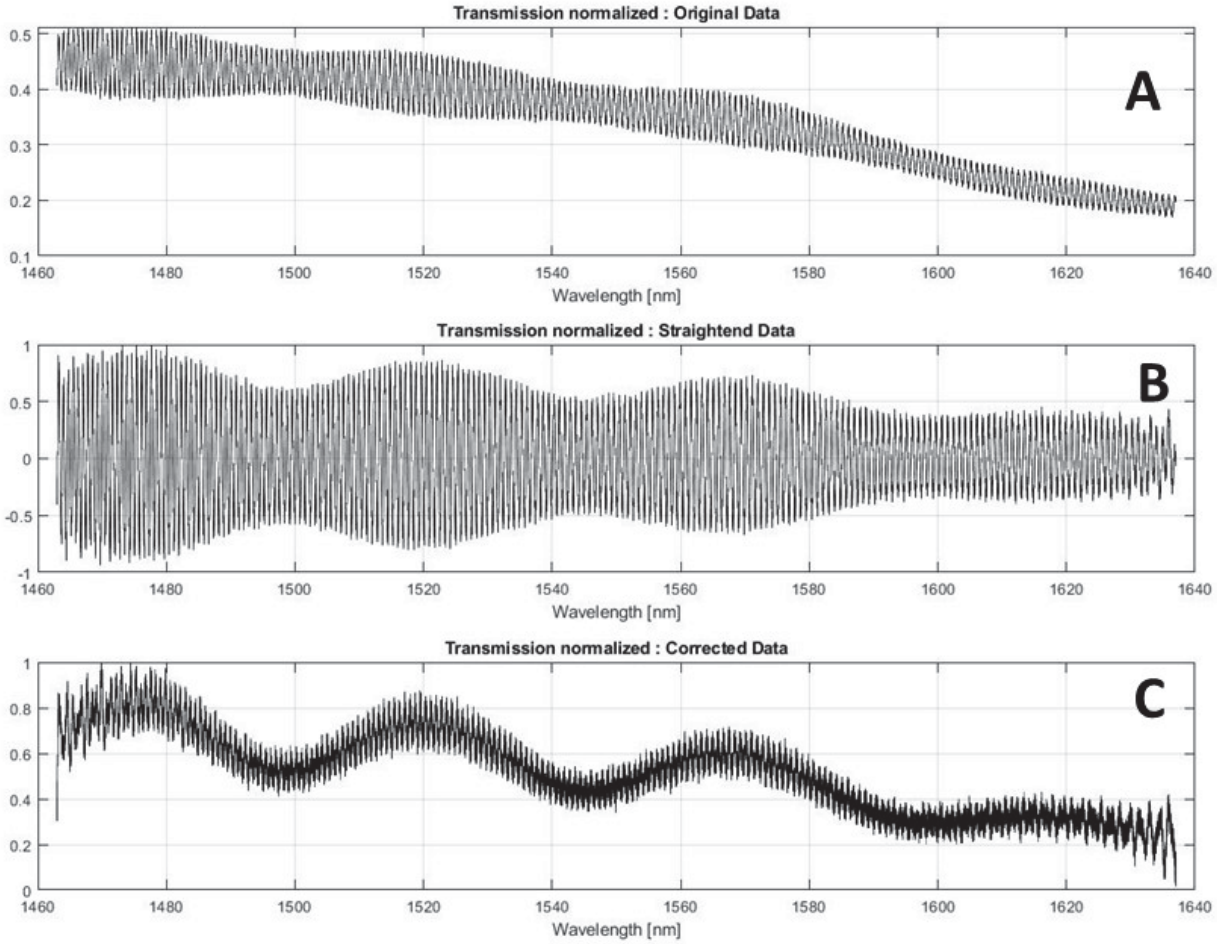

Figure 20: Transmission Spectrum of the VCSEP Device
(a) The as-measured, transmittance vs wavelength; (b) Spectra-normalized data; (c) A Hilbert Transform showing the VCSEP response with the expected free-spectral range.

The single VCSEP device can be considered as a sequence of Fabry-Perot resonators with three different resonators defined in the VCSEP cross section as explained in Figure 21. The first one consists of an air-silicon wafer-VCSEP resonator, the second one consists of an air-silicon wafer-air resonator and the third resonator is one of interest: the silicon wafer-VCSEP-air resonator. Identifying the resonance response of each resonator is necessary to understand the results obtained from characterizing the single VCSEP device (see Figure 20) since the optical spot size is larger than the diameter of an individual VCSEP device and, therefore, the measured result corresponds to the response of these three resonators. Further details on the response of these three resonators and their free-spectral ranges (FSRs) are depicted in Figure.22.

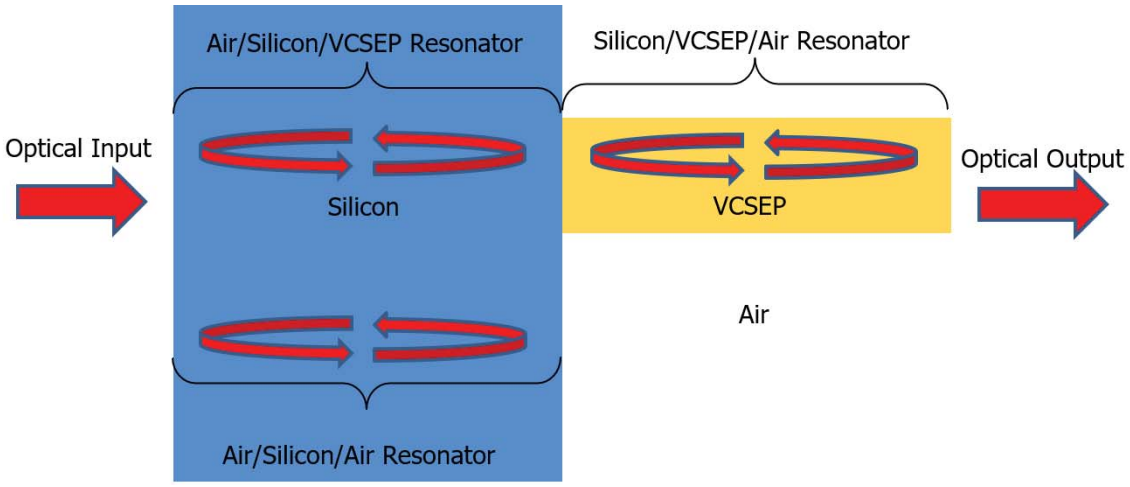

Figure 21: Cross Section Theoretical Model of the VCSEP Device

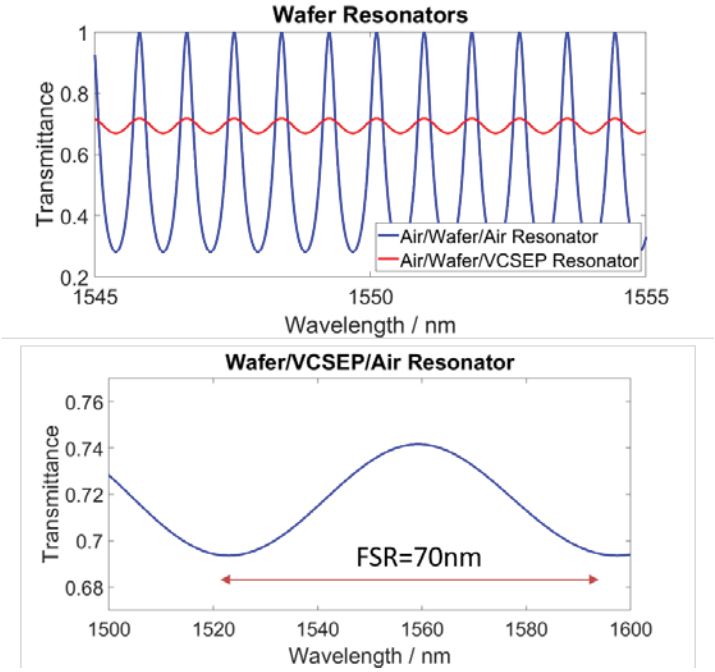

Figure 22: Theoretical Response of the Different Resonators in the VCSEP Device

With this analysis in mind, we analyzed the measured response shown in Figure 20 and derived the following observations: The transmission spectrum of the air-Si wafer-air and the air-Si wafer-VCSEP have a FSR of about 1 nm (see Figure 20a). We also need to consider the power spectra of the source and the effect of the spectra on coupling efficiency. These were taken into consideration to normalize the measured data and obtain Figure 20b. Finally, we performed a Hilbert Transform to remove the fast oscillations due to wafer resonance and obtained a curve corresponding to transmission of a single VCSEP device that is shown in Figure 20c. We estimate from the optical response of a single VCSEP device with an aspect ratio of 12.5 to have an FSR of ~45-50 nm and transmission variation of 3dB. These results confirm our design performance.

5. CONCLUSIONS

The proposed research objectives to advance the state of the art for the MOABB program by developing a VCSEP has been met. Specifically we have (i) introduced a new concept for the realization of phase shifters utilizing hybrid resonance structures in a cylindrical topology leveraging our group's prior experience in nanoscale light emitters and nanolasers; (ii) we have developed novel design and simulation tools as well as nanofabrication procedures and demonstrated devices with aspect ratios as high as 15:1 with diameters less than 1 μm (footprint <1 μm^2) enabling dense integration of VCSEP devices to achieve the ultimate goals of MOABB-wide angular scanning range (~120^o) with high resolution (~0.5^o) in 2D; (iii) we advanced the state of the art in CMOS compatible nonlinear optical materials such as silicon-rich silicon nitride for VCSEP applications. We also introduced the concept of a DC-induced Pockels effect in CMOS compatible dielectrics which will also advance numerous applications that rely on strong second-order nonlinear optical effects; (iv) we constructed two characterization and testing systems and developed novel characterization approaches that led to characterization of spectral response of single VCSEP device.

6. RECOMMENDATIONS

Based on the analysis of the current study the following recommendations for future work are offered: (i) continue investigation of the VCSEP architecture for compact integrated scanners for LIDAR applications; (ii) continue developing CMOS-compatible nonlinear optical dielectric materials exploiting the DC-induced Pockels effect for light modulation as well as nonlinear wave mixing that transfer information between different optical carrier waves. This includes the fundamental study of nonlinear optical properties of dielectrics in strong DC electric fields something easily achievable in nanoscale devices even at very low voltages.

7. REFERENCES

1. Sun, J., Timurdogan, E., Yaacobi, A., Hosseini, E. S., & Watts, M. R. (2013). Large-scale nanophotonic phased array. *Nature*, *493*(7431), 195-199
2. Xu, Q., Schmidt, B., Pradhan, S. & Lipson, M. Micrometre-scale silicon electro-optic modulator. Nature 435, 325–327 (2005)
3. Heni, W., Haffner, C., Baeuerle, B., Fedoryshyn, Y., Josten, A., Hillerkuss, D., & Dalton, L. R. (2016). 108 Gbit/s Plasmonic Mach–Zehnder Modulator with> 70-GHz Electrical Bandwidth. *Journal of Lightwave Technology*, *34*(2), 393-400.
4. Dionne, J. A., et al. "Planar metal plasmon waveguides: frequency-dependent dispersion, propagation, localization, and loss beyond the free electron model." Physical Review B 72.7 (2005): 075405.
5. Aksyuk, V. A., Dennis, B. S., Haftel, M. I., Czaplewski, D. A., Lopez, D., & Blumberg, G. (2015, June). Small footprint nano-mechanical plasmonic phase modulators. In *Solid-State Sensors, Actuators and Microsystems (TRANSDUCERS), 2015 Transducers-2015 18th International Conference on* (pp. 204-207). IEEE.
6. Melikyan, A., Alloatti, L., Muslija, A., Hillerkuss, D., Schindler, P. C., Li, J., & Chen, B. (2014). High-speed plasmonic phase modulators. *Nature Photonics*, *8*(3), 229-233.
7. Wang, Jianwei, et al. "Sub-μm 2 power splitters by using silicon hybrid plasmonic waveguides." *Optics express* 19.2 (2011): 838-847.
8. Oulton, Rupert F., et al. "A hybrid plasmonic waveguide for subwavelength confinement and long-range propagation." *Nature Photonics* 2.8 (2008): 496-500.
9. Janjan, Babak, et al. "Ultra-wideband high-speed Mach–Zehnder switch based on hybrid plasmonic waveguides." *Applied Optics* 56.6 (2017): 1717-1723.
10. M. Khajavikhan, A. Simic, M. Katz, J. H. Lee, B. Slutsky, A. Mizrahi, V. Lomakin & Y. Fainman "Thresholdless nanoscale coaxial lasers", Nature, 482, 204–207(2012)

LIST OF SYMBOLS, ABBREVIATIONS, AND ACRONYMS

ACRONYM	DEFINITION
2D	Two-Dimensional
3D	Three Dimensional
ALD	Atomic Layer Deposition
CMOS	Complementary Metal-Oxide Semiconductor
DARPA	Defense Advanced Research Projects Agency
dB	Decibel
DC	Direct Current
FDTD	Finite Difference Time Domain
FIB	Focused Ion Beam
FSR	Free-Spectral Range
LIDAR	Light Detection and Ranging
MOABB	Modular Optical Aperture Building Blocks
PECVD	Plasma-Enhanced Chemical Vapor Deposition
RF	Radio Frequency
SEM	Scanning Electron Microscope
SOI	Silicon-On-Insulator
SRN	Silicon-Rich Silicon Nitride
TE	Transverse Electric
TEM	Transmission Electron Microscope
TLM	Transfer Length Method
TM	Transverse Magnetic
USRN	Ultra-rich Silicon-Rich Silicon Nitride
VCSEP	Vertical Cavity Surface Emitting Phase-shifters